# Strongly correlated electron materials. I. Theory of the quasiparticle structure

F. López-Aguilar, J. Costa-Quintana, and L. Puig-Puig
*Departament de Física, Grup d'Electromagnetisme, Universitat Autònoma de Barcelona, Bellaterra, E-08193 Barcelona, Spain*
(Received 4 March 1992; revised manuscript receive 27 January 1993)

In this paper we give a method for analyzing the renormalized electronic structure of the Hubbard systems. The first step is the determination of effective interactions from the random-phase approximation (RPA) and from an extended RPA (ERPA) that introduces vertex effects within the bubble polarization. The second step is the determination of the density of states deduced from the spectral functions. Its analysis leads us to conclude that these systems can exhibit three types of resonances in their electronic structures: the lower-, middle-, and upper-energy resonances. Furthermore, we analyze the conditions for which there is only one type of resonance and the causes that lead to the disappearance of the heavy-fermion state. We finally introduce the RPA and ERPA effective interactions within the strong-coupling theory and we give the conditions for obtaining coupling and superconductivity.

## I. INTRODUCTION

The Hubbard model is currently used for analyzing the electronic structure of two apparently different systems, the heavy-fermion compounds[1,2] and some transition materials[3,4] such as the superconducting cuprates. We think that if we are able to analyze the conditions within the Hubbard model that lead to the different quasiparticle structure of these systems, we can better understand the electronic structure of these materials and their respective phenomenologies. The analysis of the electronic structure is carried out along the following lines: effective interaction→self-energy→spectral functions→renormalized density of states. The most simple Feynman graph series for obtaining an effective interaction is the random-phase approximation (RPA). The other more complex effective interaction worked out in this paper is determined by considering vertex effects in the bubble polarization.[5] The series defined with this effective interaction is an extension of the random-phase approximation and henceforth we term it ERPA.[6] The corresponding self-energy deduced from the different effective interactions is calculated following the so-called $GW$ approximation.[7] The self-energies calculated by using the RPA or ERPA effective interaction will be called henceforth RPA or ERPA self-energies, respectively. They lead, from a qualitative point of view, to similar spectroscopic patterns. However, the enhancement of the effective masses in the heavy-fermion state can be better obtained by the ERPA than by the RPA. The density of states (DOS) is determined from the the imaginary part of the interacting-system Green's functions, and we also obtain a self-consistent DOS. The self-consistency produces quantitative changes in the electronic structure, but maintains, from a qualitaive point of view, the same pattern for this structure.

We would like to emphasize two aspects of the electronic structure of these systems.

(i) The appearance of three features in the quasiparticle DOS (Refs. 1, 3, 8, and 9) for each state of the Hartree-Fock non-interacting system (Kampf and Schrieffer[3] and Zlatic, Ghatak, and Benermann[8] show this concept clearly). The two features at the extremes yield the upper and lower Hubbard energy bands.[1,4,8] The middle-energy resonance is responsible for the appearance of the heavy-fermion state when this resonance is such that the corresponding effective mass is largely enhanced.[1,4] It is necessary to remark that this profile with three resonances is characteristic of the electronic structure of the Ce compounds, while in U compounds it can disappear because the $5f$ band is wider than the $4f$ one.

(ii) A gradual transition takes place from a heavy-fermion state to a Hubbard state when changing the bandwidth and band occupation. In the resulting Hubbard state each strongly correlated $m$ symmetry yields a band whose location is dependent on its own occupation. Therefore, although this state has only one band for each $m$ symmetry, it also presents $m$ splitting, due to the different location of each $m$ band (see, for instance, Thalmeier and Falicov in Ref. 10 and Czycholl in Ref. 8). This result is similar to that arising from the unrestricted Hartree-Fock approximaton.

The study of the strong-coupling equations of the superconductivity can be added to the analysis of the electronic structure, considering as pair potentials interactions similar to those used for finding the self-energy. The objective of the superconductivity section is to test the possibility that a dynamical screening of the strong repulsive interaction $U$ becomes sufficient for obtaining superconductivity and to give the band conditions that make it possible.

## II. HAMILTONIAN

The many-body Hamiltonian considered in this work is the standard multiband Hubbard Hamiltonian:[11]

0163-1829/93/48(2)/1128(11)/$06.00  

$$H = H_{\mathrm{LDF}} + H_U = \sum_{\mathbf{k},\alpha} \varepsilon^0_{\mathbf{k}\alpha} n_{\mathbf{k}\alpha} + \frac{1}{2} \sum_j \sum_{m,m'} \sum_{\sigma,\sigma'} U n_{jm\sigma} n_{jm'\sigma'}, \quad (1)$$

where $H_{\mathrm{LDF}}$ is the local-density formalism Hamiltonian, index $j$ runs over all lattice sites, and $m$ and $m'$ are the symmetries of the strongly correlated orbital.

The creation operator corrresponding to $\alpha$ bands is related with the $c^\dagger_{im}$ operator by means of the relation[10]

$$c^\dagger_{jm} = \frac{1}{\sqrt{N}} \sum_{\mathbf{k},\alpha} \langle \mathbf{k}\alpha | m \rangle e^{-i\mathbf{k}\cdot\mathbf{R}_j} c^\dagger_{\mathbf{k}\alpha}, \quad (2)$$

where $N$ is the number of lattice sites. Henceforth the $m$ index includes the orbital and spin indices. The anihilation operators are related in a similar form. Equation (1) can be also written in the form of a general Hamiltonian as

$$H = \sum_{\mathbf{k},\alpha} \varepsilon^0_{\mathbf{k}\alpha} c^\dagger_{\mathbf{k}\alpha} c_{\mathbf{k}\alpha} + \frac{1}{2} \sum_{\mathbf{k},\mathbf{k}'} \sum_{\mathbf{q}} \sum_{\alpha,\beta,\zeta,\eta} \langle \mathbf{k}\alpha, \mathbf{k}'\beta | v | (\mathbf{k}+\mathbf{q})\zeta, (\mathbf{k}'-\mathbf{q})\eta \rangle \times c^\dagger_{\mathbf{k}\alpha} c^\dagger_{\mathbf{k}'\beta} c_{(\mathbf{k}'-\mathbf{q})\eta} c_{(\mathbf{k}+\mathbf{q})\zeta}, \quad (3)$$

where in our case the interaction terms, using the Hubbard approximation, are given by

$$\langle \mathbf{k}\alpha, \mathbf{k}'\beta | v | (\mathbf{k}+\mathbf{q})\zeta, (\mathbf{k}'-\mathbf{q})\eta \rangle = \frac{U}{N} \sum_{m,m'} \langle \mathbf{k}\alpha | m \rangle \langle \mathbf{k}'\beta | m' \rangle \langle m | (\mathbf{k}+\mathbf{q})\zeta \rangle \langle m' | (\mathbf{k}'-\mathbf{q})\eta \rangle = \left\langle \mathbf{k}\alpha, \mathbf{k}'\beta \left| \left( \frac{1}{N} \sum_{m,m'} |m,m'\rangle U \langle m,m'| \right) \right| (\mathbf{k}+\mathbf{q})\zeta, (\mathbf{k}'-\mathbf{q})\eta \right\rangle \quad (4)$$

with $U = \langle jm, jm' | v | jm, jm' \rangle$. The Hamiltonians (1) and (3) only differ by the constant $UN\langle n \rangle/2$, where $\langle n \rangle$ is the average occupation value of the strongly correlated orbital. The difference between $|jm\rangle$ and $|m\rangle$ is that $|jm\rangle$ is an $m$ orbital centered at $\mathbf{R}_j$, lattice site $j$, while $|m\rangle$ is a wave function centered at $\mathbf{R}_j = 0$, and it is defined by $|m\rangle = \sqrt{N}\,|0m\rangle$.

## III. DIELECTRIC FUNCTIONS

The dielectric functions corresponding to the Hamiltonian (1) and (3) can be deduced from the dynamically screened effective interactions $V(\mathbf{q},\omega)$ between states arising from localized orbitals.

The RPA can provide, at least qualitatively, the pattern of the electronic structure of the systems we treat.[3] Other diagrammatic series can yield quantitative improvements, such as, for instance the electron-hole ladder series[12] and the so-called $t$ matrix.[12,13] However, we attempt to discriminate the effects of these series both in the quasiparticle structure and in the superconductivity and therefore, in this work, we start with the RPA, which is the most simplified approximation. The RPA effective interaction $V^0(\mathbf{q},\omega)$ can be deduced from the following equation [see diagrams of Figs. 1(a) and 1(c)]:

$$\left\langle \mathbf{k}\alpha, \mathbf{k}'\beta \left| \left( \frac{1}{N} \sum_{m,m'} |m,m'\rangle V^0(\mathbf{q},\omega) \langle m,m'| \right) \right| (\mathbf{k}+\mathbf{q})\zeta, (\mathbf{k}'-\mathbf{q})\eta \right\rangle$$

$$= \left\langle \mathbf{k}\alpha, \mathbf{k}'\beta \left| \left( \frac{1}{N} \sum_{m,m'} |m,m'\rangle U \langle m,m'| \right) \right| (\mathbf{k}+\mathbf{q})\zeta, (\mathbf{k}'-\mathbf{q})\eta \right\rangle + \left\langle \mathbf{k}\alpha, \mathbf{k}'\beta \left| U\Pi^0(\mathbf{q},\omega) \left( \frac{1}{N} \sum_{m,m'} |m,m'\rangle V^0(\mathbf{q},\omega) \langle m,m'| \right) \right| (\mathbf{k}+\mathbf{q})\zeta, (\mathbf{k}'-\mathbf{q})\eta \right\rangle,$$

where

$$\Pi^0(\mathbf{q},\omega) = \frac{1}{N} \sum_{\mathbf{p},\mu,\nu} \sum_{m''} |\langle (\mathbf{p}-\mathbf{q})\nu | m'' \rangle|^2 \, |\langle \mathbf{p}\mu | m'' \rangle|^2 \left( \frac{n_{\mathbf{p}\mu}(1 - n_{(\mathbf{p}-\mathbf{q})\nu})}{\omega + \varepsilon^0_{\mathbf{p}\mu} - \varepsilon^0_{(\mathbf{p}-\mathbf{q})\nu} + i0^+} - \frac{n_{(\mathbf{p}-\mathbf{q})\nu}(1 - n_{\mathbf{p}\mu})}{\omega + \varepsilon^0_{\mathbf{p}\mu} - \varepsilon^0_{(\mathbf{p}-\mathbf{q})\nu} - i0^+} \right). \quad (5)$$

This equation is correct if the $U$ energy is independent on the $m$ and $m'$ orbitals and one supposes that each $\alpha$ band hybridizes with only one $m$ orbital. If these conditions are not valid, $V^0(\mathbf{q},\omega)$ should be obtained by a matricial treatment, since $U$ and $\Pi$ are then matrices with respect to the $m$ and $m'$ indices. $V^0(\mathbf{q},\omega)$ satisfies the equation

$$V^0(\mathbf{q},\omega) = U + U\Pi^0(\mathbf{q},\omega) V^0(\mathbf{q},\omega). \quad (6)$$

A calculation of $V(\mathbf{q},\omega)$ with ERPA can be obtained by calculating vertex effects and including them in the

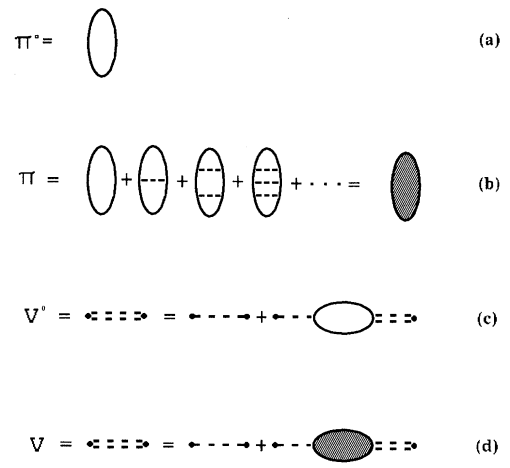


FIG. 1. Diagramatic expressions representing (a) the polarization in the RPA, (b) the polarization in the ERPA, (c) effective interaction in the RPA, and (d) the effective interaction in the ERPA.

polarization $\Pi(\omega)$ (Refs. 5 and 6) [see Figs. 1(b) and (1d)]:

$$V(\mathbf{q},\omega) = U + U\Pi(\mathbf{q},\omega)V(\mathbf{q},\omega), \tag{7}$$

where

$$\Pi(\mathbf{q},\omega) = \Pi^0(\mathbf{q},\omega) - \Pi^0(\mathbf{q},\omega)U\Pi(\mathbf{q},\omega). \tag{8}$$

The band structure $\varepsilon^0_{\mathbf{p}\mu}$ is that obtained with the local-density formalism (LDF). Due to the localization of the $m$ electrons, it is generally accepted that the effective interactions arising from the $U$ energy should depend slowly on the quasimomentum. Therefore, in Hubbard systems, the variations of these interactions versus $\omega$ are much larger than those versus $\mathbf{q}$.[8,14] We thus consider an effective screened interaction $V(\omega)$, which is the average of $V(\mathbf{q},\omega)$ over the first Brillouin zone. The suppression of the $\mathbf{q}$ dependence in the polarization is valid in the $f$ systems due to the narrowness of the $f$ bands. In the transition compounds this approximation can be discussed in some cases according to the value of the effective width of the active band near $E_F$. However, in the Y-Ba-Cu-O compounds, the bands that are close to $E_F$ present effects of strong correlation,[15] and therefore we consider that the independence of $V$ on $\mathbf{q}$ can be a reasonable hypothesis. The possible effects of the $\mathbf{q}$ dependence in this latter compound is not the purpose of the present work.

Then the RPA, ERPA, and any intermediate effective interaction between both cases can be written as

$$V(\omega) = \frac{U}{\epsilon(\omega)} = U\left[1 - U\Pi(\omega)\right]^{-1}, \tag{9}$$

where

$$\Pi(\omega) = \frac{\Pi^0(\omega)}{1 + aU\Pi^0(\omega)}, \tag{10}$$

with $\Pi^0(\omega) = \frac{1}{N}\sum_{\mathbf{q}}\Pi^0(\mathbf{q},\omega)$. For each value of the $a$ parameter, we have a different approximation for the dielectric function. For $a = 0$, the above expression corresponds to the RPA; for $a = 1$, to ERPA; and for $a = 1/2$, to the Geldart-Vosko-Hubbard (GVH) approximation to the dielectric function,[16] appropriated for extremely short-ranged bare interactions. The polarization function $\Pi^0$ can be written as $\Pi^0(\omega) = F(\omega) + F(-\omega)$, where $F(\omega)$ is given by

$$F(\omega) = \sum_m \int_{-\infty}^{0} dx \int_0^{\infty} dx' \frac{\mathcal{N}^0_m(x)\mathcal{N}^0_m(x')}{\omega + x - x' + i0^+} \tag{11}$$

and $\mathcal{N}^0_m(x)$ stands for the contribution of the $m$ orbital to the DOS in the noninteracting system.

### A. Dielectric functions in Ce systems

The DOS in the Ce systems has the following general characteristics.[8–10]

(i) The presence of two narrow and high DOS structures located very close to $E_F$. The splitting of these $f$ structures is due to hybridization with other extended states located at the same energies. In the case of the heavy-fermion state these structures can be extremely high and narrow, and the material presents a giant enhancement of effective masses ($m_{\text{eff}}$ is around 10–1000 times the free electron mass $m_0$), which brings about a very large electronic specific heat ($\gamma^*/\gamma^0 = m_{\text{eff}}/m_0$).

(ii) The Fermi level can be located on the gap or pseudogap which splits off these two structures. In some cases there is a real gap in the partial density of $f$ electrons that does not appear in the total DOS. The extended states near $E_F$ constitute a Fermi liquid which does not affect the heavy-fermion properties of the system, at least in a fundamental way.

We have developed a method in Ref. 10 in which a non-energy dependent potential arising from the Hubbard Hamiltonian is added to the LDF and we have partially obtained some of these characteristics. However, we are convinced that the electronic structure of the these Ce compounds and the enhancement of the effective mass require the introduction of the energy-dependent potentials. We choose for the DOS of the noninteracting system an analytical expression which presents similar features to those obtained in our calculations of Ref. 10, which allows us to deduce analytical expressions for $\epsilon(\omega)$ and to study its dependence on the band parameters. A first approximation to $\mathcal{N}^0(\omega)$, which is valid for the case of the Ce-based heavy-fermion metals, is[6]

$$\mathcal{N}^0(\omega) = \sum_m \mathcal{N}^0_m(\omega) = \sum_m \frac{1}{\pi}\left[\frac{K_1^m\Lambda_m}{(\omega+\lambda_m)^2+\Lambda_m^2} + \frac{K_2^m\Xi_m}{(\omega-\xi_m)^2+\Xi_m^2}\right]. \tag{12}$$

The subindex $m$ runs over all the orbitals (for instance, the $4f$ orbitals) and all spin directions. Therefore $\mathcal{N}^0_m(\omega)$ represents the partial DOS corresponding to one orbital and one spin direction. If $\Lambda_m \ll \lambda_m$ and $\Xi_m \ll \xi_m$,

then $K_1^m \simeq n_m$ (the occupation of the $m$ orbital) and $K_2^m \simeq 1 - n_m$. Then $\Pi^0(\omega)$ becomes

$$\Pi^0(\omega) \simeq \sum_m \left( \frac{n_m(1-n_m)}{\omega - \gamma_m + i\Gamma_m} + \frac{n_m(1-n_m)}{-\omega - \gamma_m + i\Gamma_m} \right), \tag{13}$$

where $\gamma_m = \lambda_m + \xi_m$ is the splitting between the two resonances and $\Gamma_m = \Lambda_m + \Xi_m$. In the Ce compounds whose $n$ electron count ($n = \sum_m n_m$) is less than or equal to 1, we can consider, for the sake of simplicity, one $m$ orbital and so $n = n_{m\uparrow} + n_{m\downarrow}$. If we deal with a non-magnetic compound ($\alpha$-$CeAl_2$, $CeRu_2$, $CeOs_2$, etc.), $n$ can be evenly divided between both spin directions and thus $n_{m\uparrow} = n_{m\downarrow}$. In a magnetic compound such as $\gamma$-$CeAl_2$, $n$ is not evenly divided between both spin directions; for instance, in this case $n = n_{m\uparrow} \approx 0.8$.

The dielectric-response function in the different approximations when one considers only one $m$ symmetry in (12) can be written as

$$\epsilon(\omega) = \frac{\omega^2 - \Omega^2}{\omega^2 - Y^2}, \tag{14}$$

where $\Omega$ and $Y$ have the following expressions in the case of a nonmagnetic Ce compound:

$$\Omega^2 = (\gamma - i\Gamma)^2 + (1-a)Un(2-n)(\gamma - i\Gamma), \tag{15}$$

$$Y^2 = (\gamma - i\Gamma)^2 - aUn(2-n)(\gamma - i\Gamma), \tag{16}$$

and for a magnetic Ce compound:

$$\Omega^2 = (\gamma - i\Gamma)^2 + 2(1-a)Un(1-n)(\gamma - i\Gamma), \tag{17}$$

$$Y^2 = (\gamma - i\Gamma)^2 - 2aUn(1-n)(\gamma - i\Gamma). \tag{18}$$

The dielectric function (14) is valid for the different approximations RPA, ERPA, and GVH, just taking the corresponding value of the $a$ parameter. Similar behavior for $\epsilon(\omega)$ has also been deduced in previous research.[17,18] The plasmon frequencies $\omega_P$, which correspond to the real part of $\pm\Omega$, play an important role within the heavy-fermion state since they correspond to collective oscillations of the electron gas of the interacting system.[17,18]

### B. Dielectric functions in high-$T_c$ superconductors

Our experience on calculating the electronic structure in high-$T_c$ superconductors by adding the Hartree-Fock self-energy to the LDF Hamiltonian[19] allows us to conclude that the resulting DOS is less abrupt and less peaked than in the heavy-fermion state. This DOS appears to be almost constant in a narrow interval around the Fermi level. This leads us to consider expressions of $\Pi^0$ deduced either with a rectangular $\mathcal{N}^0(\omega)$ or with a Lorentzian DOS [Eq. (12)] whose bandwidth is sufficiently large for simulating the electronic structure of the Y-Ba-Cu-O compounds close to the Fermi level. In the latter case one can use Eq. (14) with the appropriate band parameters. If one considers a square shape for $\mathcal{N}_m^0$ in the energy interval close to $E_F$ for each $m$ orbital, $\Pi^0(\omega)$ is

$$\begin{aligned}\Pi^0(\omega) = -\sum_m \mathcal{N}_{0m}^2 [\,&(\omega+\delta_m)\ln|\omega+\delta_m| - (\omega-\delta_m)\ln|\omega-\delta_m| \\ &-(\omega+b_m)\ln|\omega+b_m| + (\omega-b_m)\ln|\omega-b_m| - (\omega+a_m)\ln|\omega+a_m| + (\omega-a_m)\ln|\omega-a_m|] \\ &+i\pi\,\mathrm{sgn}(\omega)\sum_m \mathcal{N}_{0m}^2 \{b_m[\Theta(b_m-\omega) - \Theta(\delta_m-\omega) + \Theta(b_m+\omega) - \Theta(\delta_m+\omega)] \\ &+a_m[\Theta(a_m-\omega) - \Theta(\delta_m-\omega) + \Theta(a_m+\omega) - \Theta(\delta_m+\omega)] \\ &+\omega[\Theta(-\omega) - \Theta(b_m-\omega) - \Theta(a_m-\omega) + \Theta(\delta_m-\omega) \\ &-\Theta(\omega) + \Theta(b_m+\omega) + \Theta(a_m+\omega) - \Theta(\delta_m+\omega)]\},\end{aligned} \tag{19}$$

where $\mathcal{N}_{0m}$ is the constant density of states corresponding to the $m$ orbital, $\delta_m = \mathcal{N}_{0m}^{-1}$ is the bandwidth, $a_m = n_m\delta_m$ [$b_m = (1-n_m)\delta_m$] is the occupied (unoccupied) energy interval of the $m$ orbital, and $\Theta(x)$ is the step function. The dielectric function is then

$$\epsilon(\omega) = 1 - U\Pi^0(\omega)\,[1 + aU\Pi(\omega)]^{-1}. \tag{20}$$

This function presents similar features to those given by Eq. (14), and the evolution versus the main electronic parameters of the strongly correlated systems ($\delta$, $n$, and $U$) is also similar to that of (14).

## IV. SELF-ENERGIES

Once we have determined the screened interaction $V^0(\omega)$ and $V(\omega)$, we can deduce the self-energy for the strongly correlated systems as[6]

$$\begin{aligned}\Sigma(\mathbf{r},\mathbf{r}',\omega) &= \sum_m \Sigma_m(\omega)\phi_m(\mathbf{r})\,\phi_{m'}^*(\mathbf{r}') \\ &= \sum_m [UX + M_m(\omega)]\,\phi_m(\mathbf{r})\,\phi_{m'}^*(\mathbf{r}'),\end{aligned} \tag{21}$$

where the $\phi_m$ functions are $m$ orbitals whose radial parts can be determined by the renormalized atom approach. The meaning and the procedure for the calculation of the $X$ parameter are given in the Appendix. For each $m$ orbital $M_m(\omega)$ is determined within the $GW$ approximation[6,7] and is given by

$$\begin{aligned}M_m(\omega) = &-U\int_{-\infty}^{E_F} \frac{\mathcal{N}_m(x)dx}{\epsilon(x-\omega)} \\ &-\frac{U}{\epsilon'(-\Omega)}\int_{-\infty}^{\infty} \frac{\mathcal{N}_m(x)}{\omega - \Omega - x}dx.\end{aligned} \tag{22}$$

Here $-\Omega$ corresponds to the zero of (14) located at the upper complex half-plane. This self-energy for the dielectric function (14) takes the form

$$\Sigma_m(\omega) = U(X - n_m) + U\frac{\Omega^2 - Y^2}{2\Omega}\int_{-\infty}^{0} \mathcal{N}_m(x)\frac{1}{\omega + \Omega - x - i0^+}dx + U\frac{\Omega^2 - Y^2}{2\Omega}\int_{0}^{\infty} \mathcal{N}_m(x)\frac{1}{\omega - \Omega - x + i0^+}dx. \quad (23)$$

Here, in paper I of this series, we give an approximated version of the spectrum of the interacting system in a general case by finding the poles of the interacting-system Green's function, defined by

$$G_m(\mathbf{k},\omega) = \left[\omega - \varepsilon^0_{\mathbf{k}\alpha} - \Sigma_m(\omega)\right]^{-1}, \quad (24)$$

where $\varepsilon^0_{\mathbf{k}\alpha}$ is the noninteracting system spectrum.

The DOS of the interacting system deduced from the spectral functions corresponding to the Green's-functions (24) and $\mathcal{N}^0(\omega)$ given by Eq. (12) is

$$\mathcal{N}_m(\omega) = \frac{1}{\pi}\left(\frac{n_m[\Sigma_2(\omega) + \Lambda_m]}{[\omega - \Sigma_1(\omega) + \lambda_m]^2 + [\Sigma_2(\omega) + \Lambda_m]^2} + \frac{(1 - n_m)[\Sigma_2(\omega) + \Xi_m]}{[\omega - \Sigma_1(\omega) - \xi_m]^2 + [\Sigma_2(\omega) + \Xi_m]^2}\right), \quad (25)$$

where $\Sigma_1(\omega) = \mathrm{Re}\Sigma_m(\omega)$ and $\Sigma_2(\omega) = |\mathrm{Im}\Sigma_m(\omega)|$. The self-consistent process is suggested because the self-energy (23) depends on the DOS, which itself depends on the self-energy. The starting point (first iteration in the self-consistent process) for obtaining $\Sigma(\omega)$ consists in taking the DOS of a noninteracting system $[\mathcal{N}^0(\omega)]$ obtained with the LDF method. Considering the DOS (12) we obtain the first iteration self-energy, which is given by

$$\Sigma_m(\omega) = U(X - n_m) + U\frac{\Omega^2 - Y^2}{2\Omega}\left(\frac{n_m}{\omega + \Omega + \lambda_m - i\Lambda_m} + \frac{1 - n_m}{\omega - \Omega - \xi_m + i\Xi_m}\right). \quad (26)$$

The results obtained in the last iteration keep features similar to those of the first iteration [expression (26)], although for some initial band parameters the results of the first and last iteration can differ from a quantitative point of view.

## V. RESULTS OF THE DIELECTRIC FUNCTION AND SELF-ENERGY

We display in Fig. 2 the dielectric functions (14) for several bandwiths. These curves have similar characteristics for different values of the $a$ parameter in (15)–(18), although from a quantitative point of view there can exist appreciable differences. In Fig. 3, we plot $\epsilon_1(\omega) \equiv \mathrm{Re}\epsilon(\omega)$ deduced from Eq. (20) for different occupations of the $m$ orbital, keeping the $U$ energy and the bandwidth constant. The most important characteristic of $\epsilon_1(\omega)$, both in Figs. 2 and 3, is the existence of two zeros in the positive zone of the frequency and two others symmetrically located in the negative one. For the first zero, $\epsilon_2(\omega) \equiv \mathrm{Im}\epsilon(\omega) \neq 0$, and for the second zero, both $\epsilon_1(\omega)$ and $\epsilon_2(\omega)$ are vanishing. We just present the curves for $n \geq 0.5$, since $\epsilon(\omega)$ is invariant with respect to the change $n \to 1 - n$. These curves present the following features: (i) a minimum at frequency $\omega \simeq \delta$; (ii) the same asymptotic value $\epsilon_1(\omega) \to 1$ when $\omega \to \infty$; (iii) two cuts with the $\omega$ axis up to a critical occupation, beyond which $\epsilon_1(\omega)$ is positive for all $\omega$; and (iv) the value of

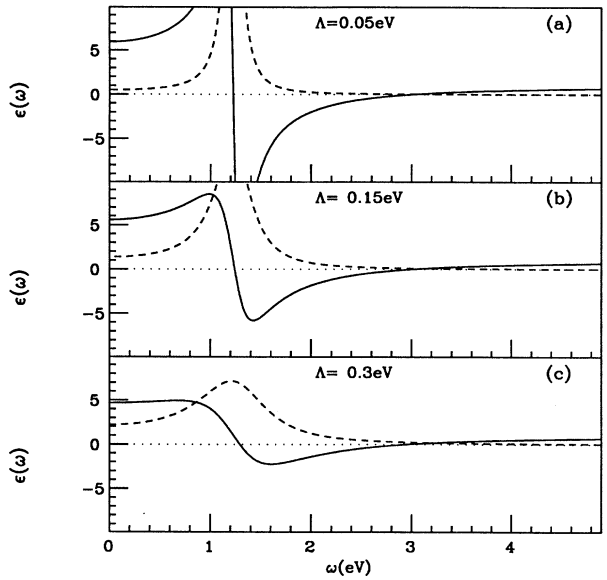


FIG. 2. Real part (solid line) and imaginary part (dashed line) of the dielectric function $\epsilon(\omega)$, obtained from Eq.(14), in the ERPA, with $U = 5.0$ eV, $\lambda = \xi = 1.5$ eV, and $n = 1/2$. (a) $\Lambda = \Xi = 0.05$ eV, (b) $\Lambda = 0.15$ eV, and (c) $\Lambda = 0.3$ eV. The factors $\Lambda$, $\Xi$, $\lambda$, and $\xi$ are defined in Eq. (12) of the text.

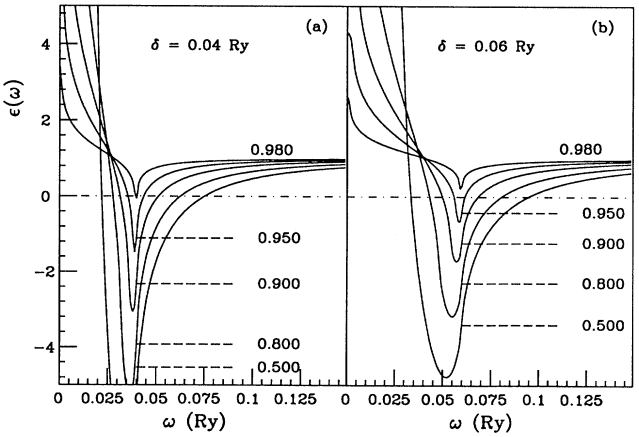


FIG. 3. Real part of the dielectric function obtained from Eq. (20) for $U = 0.5$ Ry and for different values of the $m$-electron count $n$. (a) $\delta = 0.04$ Ry and (b) $\delta = 0.06$ Ry.

the minimum of $\epsilon_1(\omega)$ decreases with $n$, and for $n$=0.5 it presents the absolute minimum of the family of curves. The evolution of $\epsilon_1(\omega)$ with $n$, keeping $U$ and $\delta$ constant, presents critical points. They correspond to occupations such that the two plasmon poles $\Omega$ and $\Omega^*$ disappear [see, for instance, Fig. 3(a) for $n$ =0.980]. These critical points imply the loss of the heavy-fermion behavior and they are found by calculating the values of $n$ for which $\epsilon_1(\omega)$ has its minima when $\epsilon_1(\omega) = 0$.

The self-energy of the first iteration is given by Eq. (26). In this paper, we consider that the $X$ parameter of (23) and (26) is canceled by $n_m$. For other values of $X$ the analysis would be the same, except for considering a $-U(X - n_m)$ translation of the $x$ axis in the figures of $\Sigma(\omega)$ versus $\omega$.

In Fig. 4 we give the results of the non-self-consistent $\Sigma_m(\omega)$ for a RPA dielectric function varying the ocupation number $n_m$. In Fig. 5, we plot the self-energy with the same parameters as in Fig. 4, but considering the ERPA dielectric functions. The comparison between Figs. 4 and 5 shows that the ERPA self-energy is qualitatively similar to RPA, although there are some quantitative differences. Figure 6 represents the self-energy in the RPA by considering the polarization function (19). One can also see that the self-energies arising from the different polarizations (19) and (13) have a similar shape considering similar bandwidths in $\mathcal{N}^0(\omega)$.

As it was explained above, the effects of the $\Sigma_m(\omega)$ potential can be analyzed by studying the poles of $G_m(\mathbf{k}, \omega)$ [Eq. (24)]. An orientative guide for the pattern of the quasiparticle spectrum can be graphically obtained from

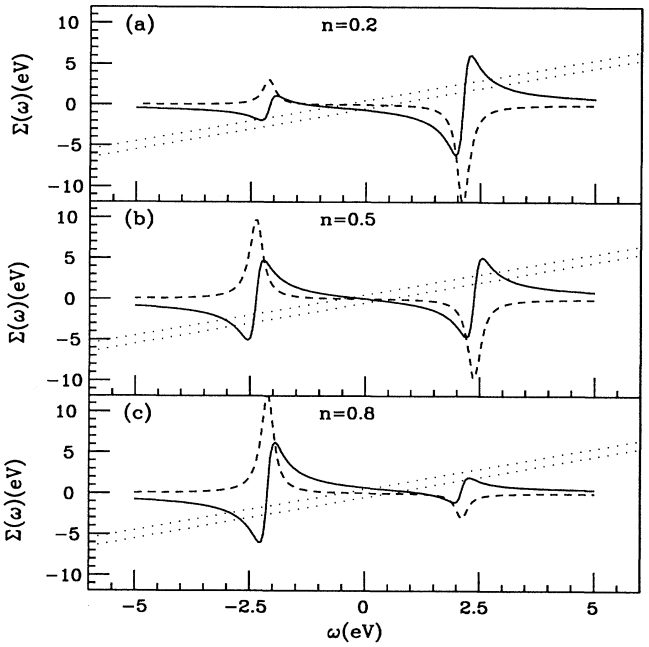


FIG. 5. Same as Fig. 4, but in the ERPA case.

the intersection of the line $y_1 = \omega - \varepsilon^0$ with the function $y_2 = \mathrm{Re}\Sigma_m(\omega)$, for each value of $\varepsilon^0$.[3] The energy range of $\varepsilon^0$ is obviously defined by the DOS, $\mathcal{N}_m^0(\omega)$. Each state in the noninteracting system arising from a partially occupied $m$ orbital yields five different resonances

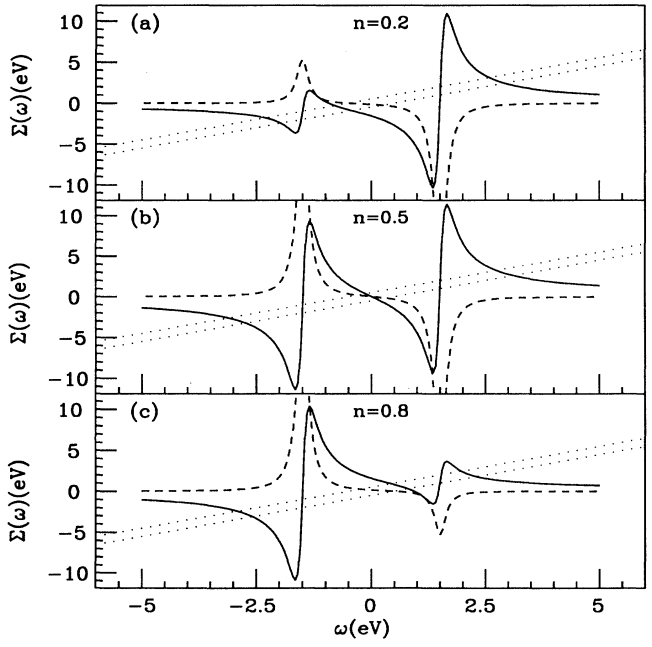


FIG. 4. Real part (solid line) and imaginary part (dashed line) of the self-energy $\Sigma(\omega)$ in the RPA case, calculated for $U$ = 5.0 eV, $\lambda = \xi$ = 0.5 eV, and $\Lambda = \Xi$ = 0.05 eV; $\Lambda$, $\Xi$, $\lambda$, and $\xi$ are defined in Eq. (12) of the text. (a) $n$ = 0.2, (b) $n$ = 0.5, and (c) $n$ = 0.8. Dotted lines represent the function $y = \omega - \epsilon^0$, where $\epsilon^0 = \pm\lambda$.

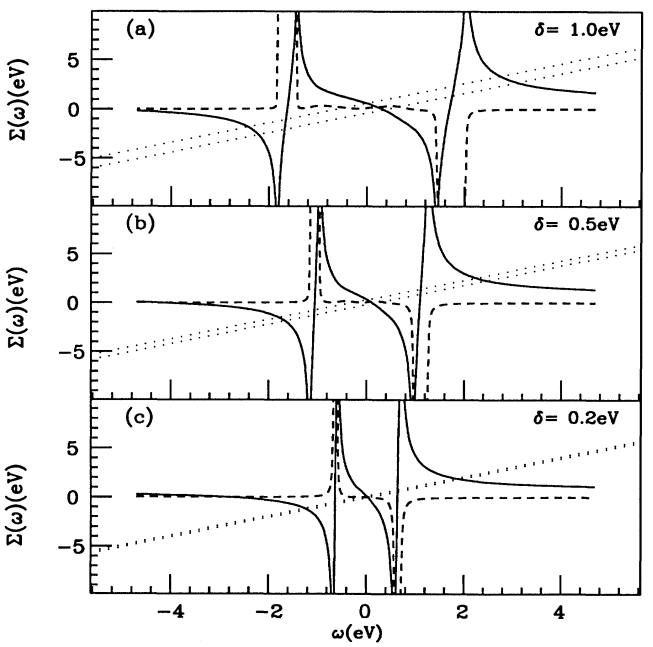


FIG. 6. Real part (solid line) and imaginary part (dashed line) of the self-energy obtained with the polarization (19), for $U$ = 6.8 eV and $n$ = 0.4, varying the bandwidth $\delta$: (a) $\delta$ = 1.0 eV, (b) $\delta$ = 0.5 eV, and (c) $\delta$ = 0.2 eV. Dotted lines represent the function $y = \omega - \epsilon^0$, $\epsilon^0$ being $-n\delta$ and $(1-n)\delta$, i.e., the ends of the band $\mathcal{N}_0$ .

(or structures) associated with the five different cuts of $y_1$ and $y_2$ (see Figs. 4 and 5). This result is also obtained in Ref. 3, whose concurrence is there named "pseudogap regime."

For a value of $n_m = 1/2$, the location of the peaks in the DOS is symmetric with respect to the third cut, which is located close to $E_F$. This cut becomes to be called Kondo $f$ peak, because its location with respect to $E_F$ determines the Kondo temperature. Our results are in agreement with Joyce *et al.*[20] in the sense that the $f$ structure close to $E_F$ is due to the screening arising from many-body effects taken into account by the dielectric response. In our case the location of this central structure is nearly the same in all approximations for $V(\omega)$. The second and fourth cuts of the pseudogap regime correspond to resonances whose half-life, defined by the inverse of $\mathrm{Im}\Sigma_m(\omega)$, almost vanishes, since the imaginary part of the self-energy is very large at these two energies (this result is in agreement with that of Ref. 3). Therefore, the Green's-function poles associated with the first, third, and fifth cuts are those that correspond to the three peaks of the DOS of the interacting system in the pseudogap regime. This is for each stationary state arising from the partially occupied $m$ symmetry in the LDF electronic structure. The splitting between these resonances is larger for increasing values of the $U$ energy and for values of $n_m$ approaching half-occupation.

The self-consistent self-energy results are presented along with the non-self-consistent ones in Figs. 7–10 and

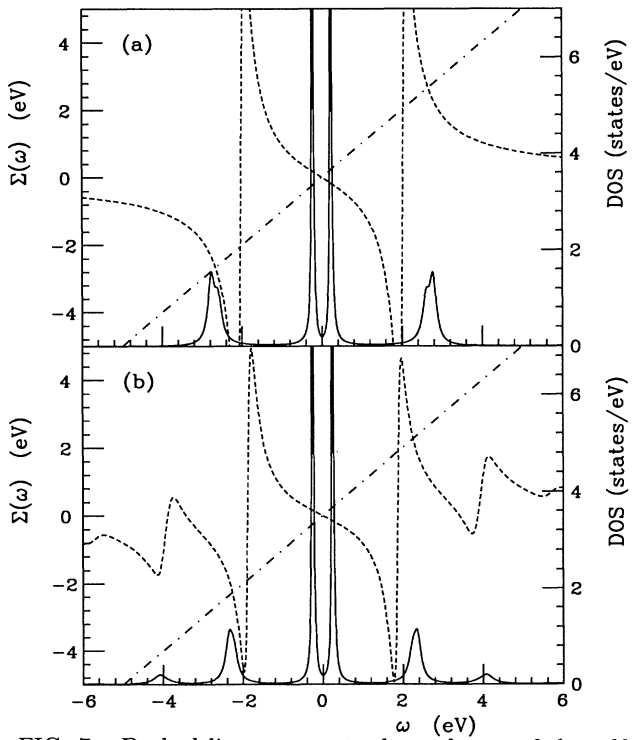


FIG. 7. Dashed line represents the real part of the self-energy in the RPA, calculated for $\Lambda = \Xi = 0.03$ eV, $\lambda = \xi = 0.4$ eV, $n = 1/2$, and $U = 5$ eV. Solid line is the resulting DOS, and the dot-dashed line corresponds to $y = \omega$. (a) Non-self-consistent calculation of the self-energy [Eq. (26)]. (b) Self-consistent calculation of the self-energy [Eq. (23)].

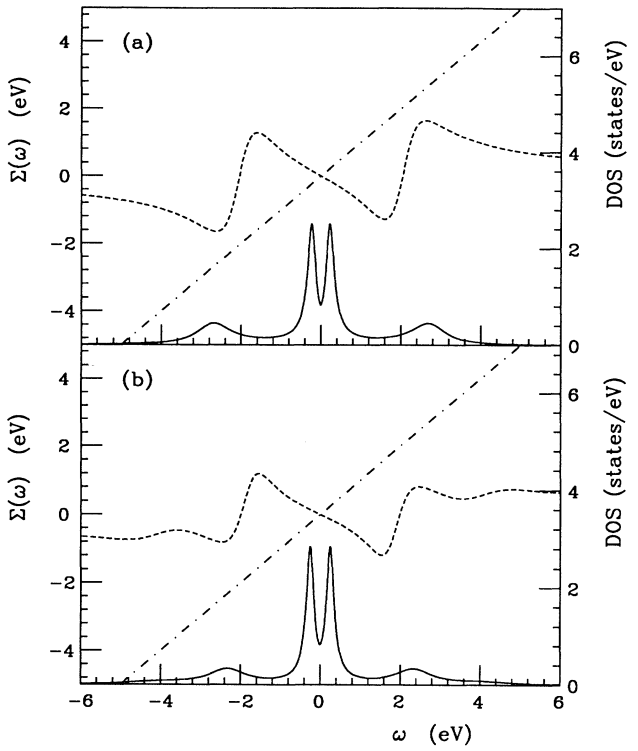


FIG. 8. Same as Fig. 7, but calculated with the following parameters: $\Lambda = \Xi = 0.15$ eV, $\lambda = \xi = 0.4$ eV, $n = 1/2$, and $U = 5$ eV. (a) Non-self-consistent calculation and (b) self-consistent one.

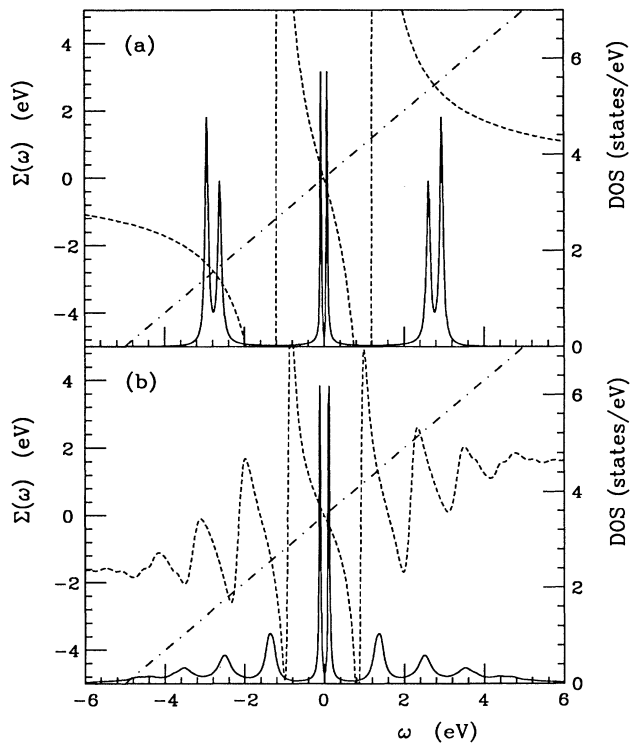


FIG. 9. Same as Fig. 7 but in the ERPA case.

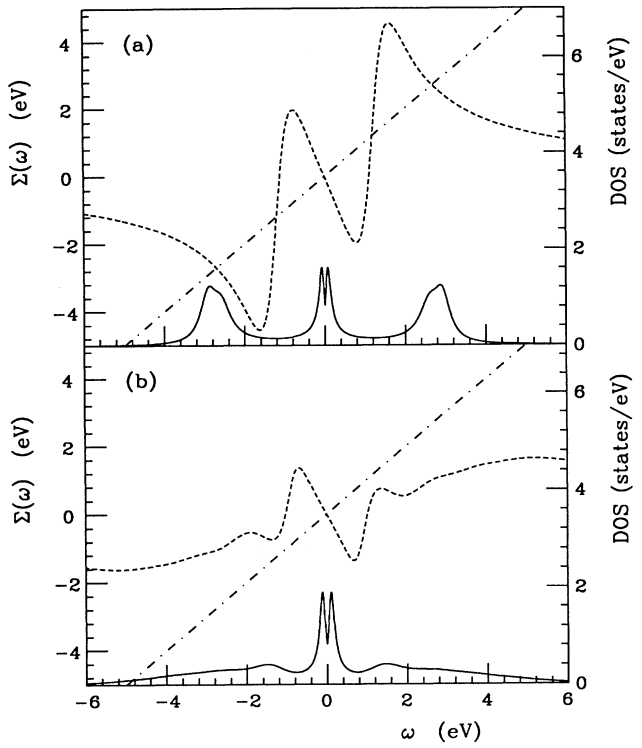


FIG. 10. Same as Fig. 8 but in the ERPA case.

seem to be in qualitative agreement with those obtained in Ref. 3. Our results present less similitude with those of Ref. 4, probably due to the fact that these authors use a nonperturbative $\frac{1}{N}$ technique, obviously different from that considered in this work. The self-consistency maintains the pattern of both the self-energy and the quasiparticle DOS, since there are also the central double structure and the lower and upper Hubbard structures. One difference is that the height of the main resonances decreases with the iterative process. This decrease of the peak height in the self-consistent DOS is more important in the ERPA than in the RPA. Another effect given by the self-consistency is the possible appearence of multipeaks in the DOS. This effect is more clear in the results performed with the ERPA; see Fig. 9(b). However, these oscillations disappear in the realistic cases via hybridization with more extended states. The splitting of the two peaks that we identify with the upper Hubbard band and lower Hubbard band in the DOS is approximately $U$ in the RPA calculation and smaller in the ERPA. The central $m$ structure can be split off in two $m$ substructures by a pseudogap. This pattern was schematically suggested by Martin's model (see Ref. 8) for compounds with a partially occupied $m$ orbital and corresponds to the so-called multipeaked $m$ structure, which is obtained in other previous papers,[3,4,8] and has been experimentally detected in a great number of experimental results.[9]

## VI. GENERAL QUASIPARTICLE STRUCTURE OF THE HUBBARD SYSTEMS

The spectrum given by the RPA approximation to the dielectric function is similar to that deduced by the ERPA, mainly the self-consistent results [see Figs. 7(b), 8(b), 9(b), and 10(b)]. We wish to emphasize that the result of three resonances, for each state of the noninteracting system, is for each of the $(2l+1)$ $m$ symmetries belonging to a given $l$ Hilbert subspace. The hybridization and the existence of several partially occupied $m$ orbitals can imply the appearance of a larger number of resonances in the total DOS. On the other hand, the presence of other extended states belonging to the noncorrelated electron sea can partially hide the peaks in the DOS arising from these resonances.

It is impossible to obtain these three DOS peaks from mean-field approximations, and they can be physically interpreted as follows. The upper-energy resonance (UER) constitutes the upper Hubbard band.[3,21] This UER could be interpreted as a band of states arising from the transition $4f^1 + e^- \rightarrow 4f^2$ that is propagated by the crystal with a definite $\mathbf{k}$. The lower-energy resonance (LER) constitutes the standard lower Hubbard band.[21] The most interesting feature is the occurrence of middle-energy resonances (MER), since they are located near $E_F$ and therefore all physical properties are dependent on them.[1,3,4,6,8] Making a logical conceptual interpolation between the UER and the LER, the MER corresponds to intermediate dynamical occupations between the resonances of extreme energies.

The heavy-fermion state arises when the middle-energy resonance presents large effective masses. In the Ce systems this feature coincides with the existence of a multipeaked structure for each partially occupied $m$ orbital.[8,9] These two characteristics are gradually lost when the band parameters of the interacting strongly correlated electron gas are modified. By regarding the solutions of equation $\omega - \varepsilon^0_{\mathbf{k}\alpha} - \Sigma(\omega) = 0$, there is a transition from five cuts to only one for a certain interval of the band parameters (compare Figs. 7 with 8 and 9 with 10). However, this transition is reflected in the DOS as a smooth and gradual change of its structure because of the gradual variation of the spectral functions on the band parameters. This transition is named in previous literature[3] as a transition from pseudogap regime to Fermi-liquid regime, and it is obvious that the pseudogap regime favors the appearance of the heavy-fermion state.[4] The main band parameters which govern the necessary changes in the self-energy for which the heavy-fermion characteristics do not appear are the $m$ occupation and mainly the width of the effective band arising from this $m$ orbital. An analysis of this evolution has been performed, and the results are displayed in Figs. 7–10. Figures 7 and 8 show this evolution within the RPA and Figs. 9 and 10 correspond to the same calculations performed within the ERPA.

Figures 7 and 9 present the characteristic pattern of the Ce systems. This case constitutes a candidate for being a heavy-fermion system. From comparison of Figs. 7 with 8 and 9 with 10, one can deduce that for increasing values of the effective bandwidth the upper and lower energy resonances almost disappear and the resulting electronic structure is a Hubbard state in which each strongly correlated $m$ symmetry yields a middle-energy resonance band whose location is dependent on its own occupation. This state presents characteristics similar to that of the

Fermi-liquid regime in previous literature.[3,4] This multiband Hubbard state, although it has only one resonance for each $m$ symmetry, can also present multiple splitting if there are different $n_m$ occupations, since the expressions of the self-energy (23) and (26) are practically reduced to $U(X - n_m)$ for a sufficient large bandwidth.

## VII. STRONG-COUPLING EQUATIONS

In this section, we include an effective interaction of the type (9) between fermions in the strong-coupling superconductivity equations for testing the possibility that this kind of interaction can produce coupling and superconductivity as it has been suggested previously.[23] This objective is similar to that of Norman's works,[2] where he analyzes the possibility of explaining the heavy-fermion superconductivity from Eliashberg equations. The effective pair potential deduced from the dielectric functions (14) and (20) produces an attractive interaction, and therefore coupling, between holes of the corresponding $m$ orbital in a frequency interval defined by $Y \leq \omega \leq \Omega$ (see Figs. 2 and 3). The reasons for assuming the independence of the $\mathbf{q}$ momentum are the same as those given in Sec. III, this condition having been considered in several previous papers.[22,24,25] The limits, $Y$ and $\Omega$, of this interval are decisive for the coupling potential to be able to produce superconductivity. The self-energies for pairs $W(\omega)$ and fermions $S(\omega)$ in the superconducting state, considering the pair potential (14), can be obtained after some mathematical manipulations[26] and their expressions are

$$W(\omega) = -\int_{-\infty}^{\infty} \frac{d\omega'}{2\pi} U\mathcal{N}_0 \left[ \sum_{\Omega} \frac{1}{\epsilon'(\Omega)} \frac{n_B(\Omega)}{\omega + \Omega - \omega'} - \frac{n_F(\omega')}{\epsilon(\omega' - \omega)} \right] \times \mathrm{Re}\left[ \frac{W(\omega')\mathrm{sgn}(\omega')}{\sqrt{\omega'^2 Z(\omega')^2 - W(\omega')^2}} \right], \tag{27}$$

$$\omega[1 - Z(\omega)] = \int_{-\infty}^{\infty} \frac{d\omega'}{2\pi} U\mathcal{N}_0 \left[ \sum_{\Omega} \frac{1}{\epsilon'(\Omega)} \frac{n_B(\Omega)}{\omega + \Omega - \omega'} - \frac{n_F(\omega')}{\epsilon(\omega' - \omega)} \right] \times \mathrm{Re}\left[ \frac{\omega' Z(\omega')\mathrm{sgn}(\omega')}{\sqrt{\omega'^2 Z(\omega')^2 - W(\omega')^2}} \right], \tag{28}$$

where $n_F$ and $n_B$ are the occupation numbers for fermions and bosons and $\Omega$ are the zeros of the dielectric function. $\mathcal{N}_0$ is the DOS, here considered as constant in a certain interval around $E_F$. $W(\omega)$ is related to the superconducting gap $[\Delta(\omega)]$ by means of the expression $W(\omega) = \Delta(\omega)Z(\omega)$. $Z(\omega)$ represents the renormalization factor and is an even function of the frequency $\omega$, defined by the self-energy by $S(\omega) = S_e(\omega) + \omega\,[1 - Z(\omega)]$, with $S_e(\omega)$ the even part of $S(\omega)$ with respect to $\omega$.

Equations (27) and (28), valid for any screening function, are solved self-consistently by an iterative process. The final result of $\Delta(\omega)$ converges either to zero, $\Delta(\omega) \to 0$, or, depending on the $\Omega$, $Y$ and $U$ values, to a function whose typical shape can be seen in Fig. 11. In the first case, one should interpret that superconductivity is not possible for these values of the electronic structure parameters, and this is the result for most of the cases. In the cases in which superconductivity is present the curves of $\Delta(\omega)$ have three characteristic features (see Fig. 11): (i) In a frequency interval $-\omega_0 < \omega < \omega_0$, $\mathrm{Re}\Delta(\omega)$ is positive, while for $|\omega| > \omega_0$, $\mathrm{Re}\Delta(\omega)$ is negative, and for $|\omega| > \omega_c$ it tends asymptotically to a small negative and constant value; (ii) for increasing temperatures, $\mathrm{Re}\Delta(\omega)$ conserves its shape but it decreases for all $\omega$ values, also for $\omega = 0$; and (iii) $T_c$ is defined as the temperature at which $\Delta(\omega)$ tends to zero for all $\omega$. These three features appear in all strong-coupling superconductors[26] and also in our calculation. $T_c$ varies linearly versus $U\mathcal{N}_0$ for the range of values of the plasmon pole $\Omega$ and $Y$ for which superconductivity is possible. In Fig. 12 we give the evolution of the $T_c$ versus the value of the $U$ parameter considering $\mathcal{N}_0$ constant. We have performed the calculation for different values of the frequency interval where the pair potential produces coupling. The transition temperature largely increases for increasing values of

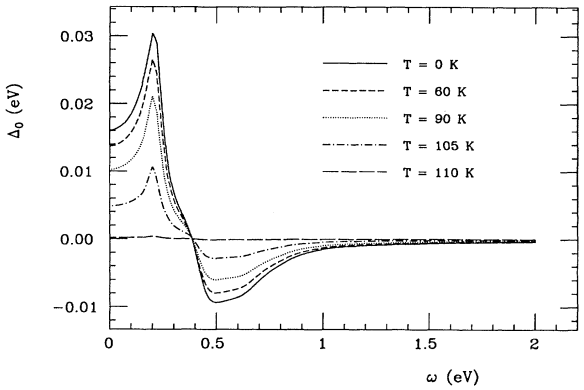


FIG. 11. Evolution of $\Delta(\omega)$ with the temperature, using the following values of the parameters: $\Omega = 0.2 - 0.03i$ eV, $Y = 0.1 - 0.005i$ eV, and $U = 6$ eV.

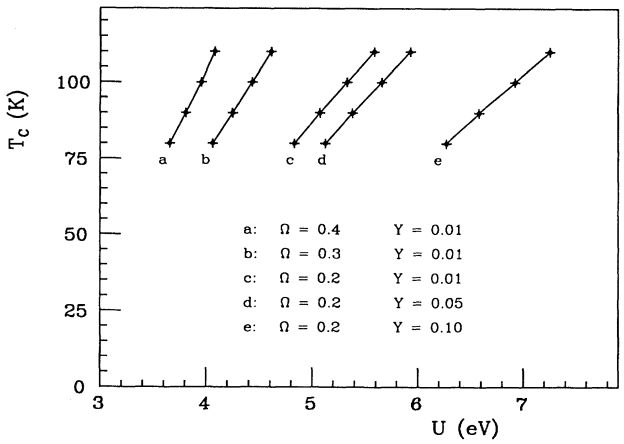


FIG. 12. Variation of $T_c$ as a function of $\mathrm{Re}\Omega$, $\mathrm{Re}Y$, and $U$. Solid lines are only a guide for the eyes.

Re$\Omega$ and decreasing values of Re$Y$. In addition, Fig. 12 shows that $T_c$ is extremely sensitive to changes of $\Omega$ and $Y$, which are dependent on the band parameters. However, these results can be taken into account only from a qualitative point of view, since, as it is known,[24,27] the RPA screening tends to overestimate $T_c$. Other types of screening functions should be included in Eqs. (27) and (28) in order to consider the results quantitatively.

## VIII. SUMMARY AND CONCLUDING REMARKS

Different approximations to the dielectric function and to the self-energy of the strongly correlated systems have been constructed, starting from a LDF noninteracting system. The infinite series of the RPA, ERPA, and GVH approximations have been considered for determining the corresponding dielectric functions. The *GW* theory concerning the self-energy has been used to determine the Green's function of the interacting quasiparticle system. An analysis of the evolution of the dielectric functions and the self-energy versus the band parameters has been performed, and the main conclusions are the following.

(i) For a narrow-band condition and/or for $n_m$ close to the half-occupation, the interacting quasiparticle gas presents a DOS with three finite lifetime resonances for each state of the noninteracting system. They can hybridize with other extended states.

(ii) For gradual increases of the bandwidth and/or for $n_m$ occupation close to 0 or 1, the heights of the corresponding resonances of the interacting system decrease and the two resonances at the extremes can even disappear. This means that the interacting system can transit to a Fermi-liquid regime.

(iii) The pattern of three resonances in the interacting system can coexist with a heavy-fermion state if the renormalization factors for energies close to $E_F$ are sufficiently large. In the cases with only one resonance in the interacting system, the multiple splitting of the different symmetries of the same strongly correlated orbital is caused because each symmetry is located according to its own occupation.

On the other hand, we have analyzed the strong-coupling equations using the effective interactions (9) as pair potentials, and we have found coupling and superconductivity for a large range of strongly correlated systems.

## ACKNOWLEDGMENTS

This work has been financed by the CICYT (Research Project Nos. MAT89-0675 and MAT91-0955) and the MIDAS program of Spain. One of us (L.P.P.) acknowledges support from the Ministerio de Educación y Ciencia of Spain.

## APPENDIX

The electronic structure of the noninteracting system, which is used for obtaining the self-energy, is that arising from the LDF calculation. The Schrödinger-like equation to solve for determining the spectrum of the interacting system in the realistic cases is (in the cases analyzed in paper II of this series we solve this equation)

$$\left[-\nabla^2 + V^n_{\mathrm{MT}}(\mathbf{r})\right]\varphi_{\mathbf{k}\alpha}(\mathbf{r}) + \int \Sigma(\mathbf{r},\mathbf{r}',\varepsilon_{\mathbf{k}\alpha})\varphi_{\mathbf{k}\alpha}(\mathbf{r}')d^3r' = \varepsilon_{\mathbf{k}\alpha}\varphi_{\mathbf{k}\alpha}(\mathbf{r}), \quad \text{(A1)}$$

where

$$\Sigma(\mathbf{r},\mathbf{r}',\omega) = \sum_m \left[UX + M_m(\omega)\right]\phi_m(\mathbf{r})\,\phi^*_{m'}(\mathbf{r}') \quad \text{(A2)}$$

and $M_m(\omega)$ is given by Eq. (22). Then the $X$ parameter of the above equation and of (23) and (26) has to be evaluated in each case, and it is deduced by means of the condition

$$UX = Un - \langle V'^{(n)}_{\mathrm{MT}}(\mathbf{r}) - V^0_{\mathrm{MT}}(\mathbf{r})\rangle, \quad \text{(A3)}$$

where $V'^{(n)}_{\mathrm{MT}}(\mathbf{r})$ is a local muffin-tin potential of the crystal constructed considering the direct interactions (but not the exchange interaction) between $n$ electrons in the strongly correlated orbital. $V^0_{\mathrm{MT}}(\mathbf{r})$ is the same potential considering $n = 0$ electrons in the $m$ orbitals. The average values of these potentials are calculated in the $m$ orbitals. The muffin-tin potential $V^n_{\mathrm{MT}}(\mathbf{r})$ of (A1) contains both the interactions of $V'^{(n)}_{\mathrm{MT}}(\mathbf{r})$ and also the exchange interaction corresponding to the $n$ strongly correlated electrons. Theoretically, the value of $UX$ should be close to zero, since $Un$ is the direct first-order diagram with the $U$ interaction and the difference between the potentials $V'^{(n)}_{\mathrm{MT}}(\mathbf{r})$ and $V^0_{\mathrm{MT}}(\mathbf{r})$ represents this term within the LDF approximation. However, the $U$ energy is a many-body parameter, so one usually takes an experimental result, while the potentials $V^n_{\mathrm{MT}}(\mathbf{r})$, $V'^{(n)}_{\mathrm{MT}}(\mathbf{r})$, and $V^0_{\mathrm{MT}}(\mathbf{r})$ are obtained by means of a self-consistent calculation within the local-density formalism. The direct interactions included in the muffin-tin potentials are just the interelectronic Coulombian repulsion potential deduced by means of the Hartree equation by considering a self-consistently obtained density of charge. The exchange interactions between the $n$ electrons of the $m$ orbitals are taken into account by means of an exchange parametrized potential included in $V^n_{\mathrm{MT}}(\mathbf{r})$, which already considers many-body effects. Therefore, to avoid repetitions in the electron-electron interactions considered in the self-energy, we only consider the RPA diagrams without the so-called exchangelike RPA diagrams. However, we recognize that the evaluation of the incidence of the different LDF potential contributions in the process for obtaining the self-energy is an open question.

[1]See, for instance, M.M. Steiner, R.C. Albers, D.J. Scalapino, and L.J. Sham, Phys. Rev. B **43**, 1637 (1991), and references therein; Y. Meir, N.S. Wingreen, and P.A. Lee, Phys. Rev. Lett. **66**, 3048 (1991).

[2]M. Norman, Phys. Rev. Lett. **59**, 232 (1987); Phys. Rev. B **37**, 4987 (1988).

[3]A. Kampf and J.R. Schrieffer, Phys. Rev. B **41**, 6399 (1990); **42**, 7967 (1990).

[4]H. Kim and P.S. Riseborough, Phys. Rev. B **42**, 7975 (1990).
[5]E.L. Shirley, L. Mitáš, and R.M. Martin, Phys. Rev. B **44**, 3395 (1991).
[6]S. Balle, F. López-Aguilar, and J. Costa-Quintana, Phys. Rev. B **41**, 8672 (1990).
[7]L. Hedin and S. Lundqvist, Solid State Phys. **23**, 1 (1969); G.D. Mahan and B.E. Sernelius, Phys. Rev. Lett. **62**, 2718 (1989).
[8]See, for instance, R.M. Martin, Phys. Rev. Lett. **48**, 362 (1982); V. Zlatic, S.K. Ghatak, and K.H. Benermann, *ibid.* **57**, 1263 (1986); C. Czycholl, Phys. Rep. **143**, 277 (1986); P. Schlottmann, *ibid.* **181**, 3 (1989).
[9]See, for instance, J.W. Allen, S.J. Oh, I. Lindau, J.M. Lawrence, L.J. Johansson, and S.B. Hagstrom, Phys. Rev. Lett. **46**, 1100 (1981); Y. Baer, H.R. Ott, J.C. Fuggle, and L.F. de Long, Phys. Rev. B **24**, 5384 (1981); E.Wuillord, H.R. Moser, W.D. Scheneider, and Y. Baer, *ibid.* **28**, 7354 (1983); D.M. Wieliczka, C.G. Olson, and W. Linch, Phys. Rev. Lett. **52**, 2180 (1984); Phys Rev. B **29**, 3028 (1984); J.S. Kang *et al.*, *ibid.* **41**, 6610 (1990); W.P. Beyermann *et al.*, Phys. Rev. Lett. **66**, 3289 (1991); S.K. Malik and D.T. Adroja, Phys. Rev. B **43**, 6277 (1991).
[10]P. Thalmeier and L.M. Falicov, Phys. Rev. B **20**, 4637 (1979); F. López-Aguilar, S. Balle, and J. Costa-Quintana, *ibid.* **38**, 163 (1988).
[11]A.K. Mahan, R.M. Martin, and S. Satpathy, Phys. Rev. B **38**, 6650 (1988).
[12]J.A. White, Phys. Rev. B **45**, 1100 (1992).
[13]S. Doniach and S. Engelsberg, Phys. Rev. Lett. **17**, 750 (1966).
[14]C.M. Varma, Phys. Rev. Lett. **55**, 2723 (1985).
[15]T. Takahashi *et al.*, Phys. Rev. B **39**, 6636 (1989).
[16]G. D. Mahan, *Many Particle Physics* (Plenum, New York, 1981); T. Büche and H. Rietschel, Phys. Rev. B **41**, 8691 (1990).
[17]W.P. Beyermann, G. Gruner, Y. Dalichaouch, and M.B. Maple, Phys. Rev. Lett. **60**, 216 (1988); Phys. Rev. B **37**, 10 353 (1988).
[18]P. Coleman, Phys. Rev. Lett. **59**, 1026 (1987).
[19]J. Costa-Quintana, F. López-Aguilar, S. Balle, and R. Salvador, Phys. Rev. B **39**, 9675 (1989).
[20]J.J. Joyce *et al.*, Phys. Rev. Lett. **68**, 236 (1992).
[21]P.W. Anderson, Int. J. Mod. Phys. B **2**, 181 (1990); N.F. Mott, Rep. Prog. Phys. **47**, 909 (1984).
[22]F. Mila and E. Abrahams, Phys. Rev. Lett. **67**, 2379 (1991).
[23]C.M. Varma *et al.*, Phys. Rev. Lett. **63**, 1996 (1989).
[24]M. Grabowski and L.J. Sham, Phys. Rev. B **29**, 6132 (1984).
[25]F. López-Aguilar and J. Costa-Quintana, Int. J. Mod. Phys. B **6**, 2375 (1992).
[26]D.J. Scalapino, J.R. Schrieffer, and J.W. Wilkins, Phys. Rev. **148**, 263 (1966); W.L. McMillan, *ibid.* **167**, 331 (1968).
[27]N.E. Bickers, D.J. Scalapino, and S.R. White, Phys. Rev. Lett. **62**, 961 (1989).